DOI: 10.1021/ma902542e

Macromolecules
ARTICLE

Combined SANS, SEC, NMR, and UV−vis Studies of Simultaneous Living Anionic Copolymerization Process in a Concentrated Solution: Elucidation of Building-Up Processes of Molecules and Their Self-Assemblies

Yue Zhao, Nobuyoshi Miyamoto,† Satoshi Koizumi,* and Takeji Hashimoto*

Advanced Science Research Center (ASRC), Japan Atomic Energy Agency (JAEA), Tokai, Ibaraki 319-1195, Japan. † *Present address: Department of Life, Environment, and Material Science, Faculty of Engineering, Fukuoka Institute of Technology, 811-0295 Fukuoka, Japan.*

Received November 17, 2009; Revised Manuscript Received February 2, 2010

ABSTRACT: A simultaneous living anionic copolymerization of a concentrated solution of deuterated styrene (S) and nondeuterated isoprene (I) monomers in deuterated benzene as a solvent was studied by a combination of time-resolved measurements of small-angle neutron scattering (SANS), size exclusion chromatography (SEC), nuclear magnetic resonance (NMR), and ultraviolet−visible spectroscopy (UV−vis). The molecular building-up process and its consequence on the bottom-up self-assembling process during the copolymerization reaction were observed on three different length scales on the same batch of the solution, which enabled us to explore simultaneously the time changes in the local structure (living chain ends), the primary structure (propagating chains), and the higher order structure (microdomains). We found that the copolymerization process was divided into two time regions, defined by regions I and II. In region I, the copolymerization of S and I monomers took place, and all I monomers were consumed at the end of region I. In the early stage of region I (region I_a), the SANS profiles were almost time-independent and exhibited no scattering maximum, whereas in the late stage of region I (region I_b), a scattering maximum appeared at q_m and hardly changed with time, although the maximum intensity I_m slightly increased with time. In region II, pure polystyrene (PS) block chains were formed. q_m and I_m rapidly decreased and increased, respectively, and the polymerization-induced disorder−order transition (ODT) and order−order transition (OOT) were observed. The living polymers having isoprenyl anion at the chain end (denoted hereafter by PI) started to change into those having styryl anion at the chain end (denoted hereafter by PS), and hence the polymerization of S monomers occurred under the coexistence of PI^- and PS^-. As a consequence, we found an increase in the polydispersity index of the molecular weight, M_w/M_n, and a slower effective reaction rate of S monomers relative to the corresponding homopolymerization of S monomers.

I. Introduction

In our previous study,[1] we reported a simultaneous living anionic copolymerization in a concentrated solution of deuterated styrene (S) and nondeuterated isoprene (I) monomers in deuterated benzene (benzene-d_6) as a nonpolar solvent and *sec*-butyllithium (*sec*-BuLi) as an initiator. The prescribed system had a very concentrated solution of monomers (∼50 wt %) such that the solution of propagating polymer chains reached the overlapping concentration in the very early stage of polymerization, hence, causing the microphase separation during the course of the polymerization. We investigated the polymerization process by means of time-resolved (Tr) small-angle neutron scattering (SANS) and size exclusion chromatography (SEC), which were conducted separately using different batches of the same polymer solutions. We consider the results obtained therefrom to be preliminary ones because the time scales relevant to the SANS and SEC experiments on the different batches are not necessarily identical in a rigorous sense. The preliminary results lacked important information on time evolution of monomer conversion, sequence distributions of S and I, and species at the living chain ends. In this sense, too, previous results are good only as preliminary ones.

Nevertheless, the preliminary studies elucidated three different time regions (regions 1−3) in the copolymerization process. In region 1, the living polymers having both isoprenyl anion at the chain end (designated by PI^- hereafter) and styryl anion at the chain end (designated by PS^- hereafter) selectively reacted with I monomers, forming approximately a random copolymer-rich in I unit, and propagating chains were associated to form "aggregates", as evidenced by the low-q upturn in the SANS profiles. In region 2, most or all of I was consumed, and some PI^- reacted with S and changed into styryl anion; However, the propagation of chains into a long S sequence may not fully start until almost all PI^- had changed into PS^-. Therefore, in region 2, a short PS block sequence or tapered block sequence poly(I/S)$^-$ might be formed. This behavior was postulated to be explained by the presence of the aggregates in region 2, which have almost the same characteristics as those in region 1, although the postulate left unverified. In region 3, a rapid growth of PS chains was observed due to the transformation of the chain ends from PI^- to PS^-, which may drastically change the nature of the ion aggregates and strongly enhance reactivity with S. In this time region, the order−disorder transition (ODT) from the disorder state to the cylindrical microdomain structure and order−order transition (OOT) from cylindrical to lamellar structure occurred.

In this article, we aim to conduct an advanced experiment by employing simultaneous measurements of Tr-SANS, SEC, NMR

*To whom correspondence should be addressed.

 Published on Web 02/18/2010

(nuclear magnetic resonance), and UV−vis spectroscopy for the same reaction solution in a single batch. Combining the four Tr-techniques, we aim to observe the structural change of living polymer chains on three different length scales on a rigorously common time scale, for example, the changes in microscopic structural elements (i.e., the species at the living chain ends through UV−vis spectroscopy), propagating primary structure (i.e., the molecular weight and its distribution of a single chain through SEC and a sequence distribution of S and I along the chain through NMR) and a higher-order chain structure on the mesoscopic scale (i.e., nanopatterns formed due to the microphase separation of the propagating copolymer chains through SANS), and interrelationships between these structural changes. Note that clarification of the giant wormlike micelles, which has been proposed by Stellbrink et al.,[2] is not the primary objective of this study, because the SANS q range particularly set for this study was not appropriate to permit the investigation of the giant micelles.

It is reported that the reactivities between living chain ends and monomers S or I are very different in a nonpolar solvent[3]

$$k_{SI} >> k_{SS} > k_{II} > k_{IS} \quad (1)$$

where k_{AB} denotes the rate constant for propagation reaction from PA^- to PAB^- with A and B being S or I. Because of this relationship, a growing polymer spontaneously changes from polyisoprenyl anions (PI^-) to polystyryl anions (PS^-) and vice versa during the copolymerization process.[3,4] The different reactivity ratio of S and I leads to the formation of the so-called "tapered block copolymer chain",[5−9] which has a gradient of composition along the copolymer chain in either monomer: I is mainly polymerized first until its concentration becomes relatively low, whereas S starts being incorporated in the propagating polymer chains with increasing amounts as the reaction continues, and after complete consumption of I, a pure PS block is formed.

In a nonpolar solvent, the living chain ends tend to associate via electrostatic interactions.[2,10−15] By using a light scattering technique in living anionic polymerization of S to PS, Worsfold et al.[10] investigated the association behavior of living PS^-, whose living chain end is capped with isoprenyl lithium in cyclohexane, which is a nonpolar and Θ-solvent for PS at 34.5 °C. They concluded that the association number of the living chain ends, n, ranges from 2.8 to 4.1 for PS with molecular weight of (1.0 to 1.6) × 10^5. Maliakal et al.[11] addressed the issue of chain length dependence of polymer end−end reaction rates in the reaction of monodispersed polystyryllithium (PSLi) and polystyrene terminated with a reactive styrene and suggested the effects of the chain-end association on the reaction rate. Recently, the SANS technique emerges as a powerful tool for in situ observation of the living anionic polymerization process. Fetters, Richter, and coworkers[12] have reported that starlike aggregates with $n \approx 4.0$ exist during living anionic homopolymerization of I monomers in deuterated heptane. They suggested the presence of the giant wormlike aggregates also, which are higher order superstructures of the starlike local aggregates of the living chains, during living anionic homopolymerization of butadiene (B), S, or I in nonpolar solvents.[2,12−14]

Although the living anionic copolymerization of S and I has been extensively studied in the past, there have been no systematic studies that aim to investigate in situ (1) how the nanopatterns and association number of chain ends vary during the simultaneous copolymerization process of S and I monomers and (2) how the change affects the reaction itself. To address the questions raised above, it is crucial to investigate simultaneously the changes occurring in the reaction solution on both microscopic and macroscopic scales for the same reaction solution in a single batch.

We would like to stress that there have been no studies reported so far along the line, as described above, on the simultaneous living anionic copolymerization process, except one of our recent work[16] in which for the first time, the methodology of the combined Tr methods mentioned above has been applied to extract simultaneously the various fundamental quantities in a dilute solution of monomers that never caused the microphase separation. Owing to this methodology, we perfectly observed the structural change of the living chains during the polymerization process from microscopic structure to the high-order chain structure and elucidate the information transmittance among different hierarchical structure levels involved in the reaction. However, the polymerization-induced microphase separation and nanopatterns never appeared in that study because of the sufficiently dilute solution. To complete the study, we here apply the same methodology as that described above to the concentrated solution again.

II. Experimental Sections

II-1. Living Anionic Polymerization. First, 50 μL of a solution of 1.0 M *sec*-BuLi in cyclohexane and 4.6 mL of benzene-d_6 was added to the specially designed reaction vessel (details can be found in ref 16). Then, a prescribed amount of I and S monomers (3.2 and 2.2 mL, respectively) was added to the vessel to start the polymerization, such that the initial weight ratio of S, I, and benzene-d_6 is 25:25:50. Therefore, the concentration of the polymer solution obtained at the end of the polymerization, C_{final}, is calculated to be 50 wt % from the compositions of the initial solution. The reaction solution was kept at 25 °C.

To eliminate the contamination of the system with water and air during the polymerization, we designed a reaction vessel with two branches. The detailed experimental procedure could be found again in ref 16. The effective initiator concentration, $[Ini]_{eff}$, in this study was calculated to be ∼3.4 mM, whereas the theoretical initiator concentration calculated was 5 mM.[17] This means that ∼32% of the initiator was deactivated because of impurities brought about in the polymerization process in this work. Note that the neutralization of the impurities by *sec*-BuLi produces some polar compounds,[3] which could affect the chain-end association and the kinetics of the copolymerization. However, in this study, we are not going to focus on this problem.

II-2. SANS Measurement. Tr-SANS measurements were performed with SANS-J-II at research reactor JRR-3, JAEA, Tokai, Japan.[18] The incident neutron beam was monochromatized with a velocity selector to have the average wavelength (λ) of 6.5 Å with the wavelength distribution, as characterized by $\Delta\lambda/\lambda$ = 12%. During the SANS measurements, the sample solution was controlled at 25 °C with accuracy of ±0.5 °C. The scattered neutrons were detected with a 2D ^{3}He position sensitive detector. The 2D scattering patterns were circularly averaged to obtain scattering profiles as a function of q, where q is a magnitude of the scattering vector, defined by $q = (4\pi/\lambda)\sin(\theta/2)$, with θ being the scattering angle. Hereafter, we consistently used nanometers as unit of q. The obtained scattering profiles were corrected for background scattering, electronic noise of detector, detector sensitivity, and transmission and finally normalized with a porous aluminum plate, which serves as a secondary standard, to give the absolute intensity scale (cm^{-1}).[18] The incoherent scattering intensity is estimated from the scattering intensity of the same reaction solution of benzene-d_6 and initiator before polymerization, as ∼0.1 cm^{-1}. The estimated incoherent scattering was subtracted from the observed net absolute scattering intensity.

II-3. SEC and NMR Measurements. We conducted SEC (Tosoh GPC-8220 with a refractive index detector) and NMR (proton NMR spectra were recorded at a Larmor frequency of 400 MHz on a INOVA-plus, Varian Technologies, using a 5 mm high-resolution triple-resonance probe optimized for proton observation) measurements at different reaction times. Prior to SEC and NMR measurements, aliquots of the solutions were first taken up at given times from the reaction solution and

terminated by the addition of a proper amount of deuterated methanol, both processes being conducted under the flow of the dry argon gas. Then, tetrahydrofurane (THF) was used to dilute the solution to ~0.2 wt % for SEC measurements, and deuterated chloroform ($CDCl_3$) was used to make a ~0.5 wt % solution for NMR measurements.

II-4. UV−vis Spectroscopy. We measured Tr-UV−vis spectroscopy simultaneously with SANS during the polymerization process for the exactly same reaction solution, which has been described in detail elsewhere.[15,16] Two kinds of light source were used for an incident UV−vis light. One is a mercury lamp with wavelength of 190−500 nm, and the other is a tungsten/krypton lamp with wavelength of 350−1700 nm. In this study, the wavelength is selected between 190 and 600 nm. The UV−vis spectra were collected with optical fibers and a CCD type detector (StellarNet, FL, USA) and corrected for the background (quartz cell) spectrum.

The experimental details of UV studies in this system have been detailed in ref 16. Here we would like to note that UV absorbance at $\lambda = 450$ nm at a given time, t, $A_t(450)$, is selected to estimate the volume fraction of PS^- in the total anions, PS^- plus PI^-, $\phi_{PS}^-(t) = A_t(450)/A_\infty(450)$, where $A_\infty(450)$ is absorbance at the end of the reaction. Because the concentration of PS^- at the end of the reaction, $[PS^-(t = \infty)] \approx [Ini]_{eff}$ and can be estimated from the molecular weight of the polymer at the end of the polymerization and after termination,[17] one can estimate the concentration of PS^- at a given time, $[PS^-(t)]$, from the measured $\phi_{PS}^-(t)$. One can also evaluate the concentration of PI^- at a given time, $[PI^-(t)]$, by using the relation $[PS^-(t)] + [PI^-(t)] = [PS^-(t = \infty)]$.

III. Results

III-1. Time-Resolved SEC and NMR Measurements. An apparent number-averaged molecular weight of a polymer chain, $M_{n,app}$, at a given time was obtained from the SEC measurements on the basis of PS standard. The total number-average molecular weight of the polymer, the total weights of I monomeric units and S monomeric units per polymer, all at the end of the polymerization and after termination, $M_{n,final}$, $M_{n,final,I}$, and $M_{n,final,S}$ were calculated to be $\sim 1.27 \times 10^5$, 6.35×10^4, and 6.35×10^4, respectively, from the corresponding apparent total number-average molecular weight of the copolymer, $M_{n,final,app}$, as detailed in ref 19. The polydispersity index characterizing molecular weight distribution, M_w/M_n, is ~1.055 at the end of the polymerization and after termination, where M_w denotes the weight-average molecular weight of the polymer.

Because nondeuterated I monomeric units in the living polymer chains could be clearly identified by ^1H NMR spectroscopy (details can be found in ref 16), one can estimate the monomer conversions for I monomers, $C_I(t)$, as a function of time. Note that we deliberately chose spectra for polymers to calculate $C_I(t)$ to avoid effects of evaporation of I monomers during the sampling process. One can also estimate the total weight of I monomeric units per one polymer chain at a given time, $M_{n,I}(t)$, by

$$M_{n,I}(t) = C_I(t) M_{n,final,I} \quad (2)$$

The monomer conversion for deuterated S monomers as a function of time, $C_S(t)$, can be calculated from $M_{n,app}$ as

$$C_S(t) = \frac{M_{n,app}(t) - 1.6 M_{n,I}(t)}{M_{n,final,S}} \quad (3)$$

where 1.6 is a calibration factor, as described in ref 19. Therefore, the real number-average molecular weight of a polymer chain at a given time, $M_n(t)$, can be estimated from $C_I(t)$ and $C_S(t)$ as

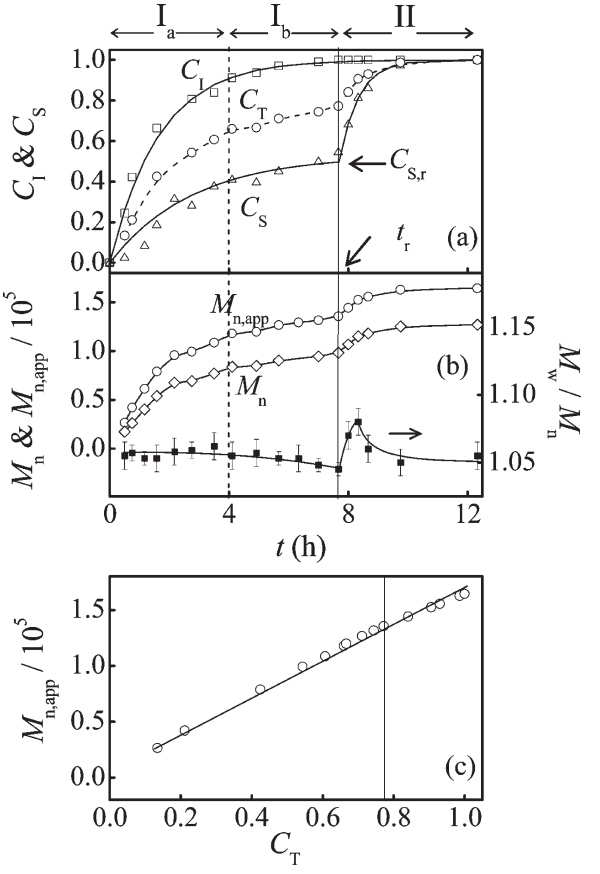

Figure 1. Time dependence of (a) monomer conversions and (b) $M_{n,app}$, M_w/M_n, and M_n. (c) $M_{n,app}$ versus the total conversion, C_T, during the living anionic polymerization process. The vertical broken line and solid line indicate the time at the end of region I_a ($t_{c,SANS} \approx 4$ h) and region I_b ($t \approx 7.8$ h), respectively. The lines drawn for $M_{n,app}$ and M_w/M_n are only for visual guides, whereas that for C_I is given by eq 6, that for C_S is given by eq 7 for region I and by eq 25 for region II, that for C_T is given by eq 5, and that for M_n is given by eq 4.

$$M_n(t) = C_I(t) M_{n,final,I} + C_S(t) M_{n,final,S} \quad (4)$$

Figure 1a shows the time dependence of $C_I(t)$ and $C_S(t)$. Their characteristic behaviors can be classified into two time regions, defined by regions I and II, as shown on the top of the Figure and as separated by the vertical solid line. In region I ($0 \le t/h \le 7.8$), $C_I(t)$ continuously increases with time, t, and reaches ~1.0 at the end of this region, whereas $C_S(t)$ increases slowly and reaches a nearly steady value of 0.5 at the end of the region. We may further divide region I into regions I_a and I_b with respect to the critical time, $t_{c,SANS}$, (the vertical broken lines), above which the SANS scattering maximum appears, as will be shown later in Figure 4. In region I_a (in early stage of region I where $t < t_{c,SANS}$), $C_I(t)$ and $C_S(t)$ rapidly increase and reach 0.9 and 0.4, respectively, in comparison with those in region I_b (a late stage of region I where $t > t_{c,SANS}$). In region II ($7.8 \le t/h \le 12$), only S monomers exist, and the consumption rate of S monomers in this region is much faster than that in region I. The broken line in Figure 1a represents the total conversion of I and S monomers, $C_T(t)$, as a function of time, t, defined by

$$C_T(t) \equiv [C_I(t) + C_S(t)]/2 \quad (5)$$

The result reveals a two-step increase in C_T with t. The characteristic time where C_I effectively reaches unity is defined by t_r ($t_r \approx 7.8$ h), and $C_S(t)$ at t_r is defined by $C_{S,r}$

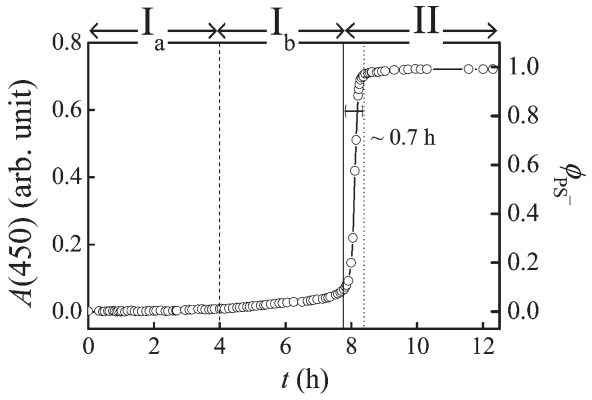

Figure 2. Time change in $A(450)$ (left ordinate axis) and ϕ_{PS^-} (right ordinate axis) during the whole polymerization process. The vertical broken and solid lines indicate the time at the end of region I_a ($t_{c,SANS} \approx$ 4 h) and region I_b ($t \approx 7.8$ h), respectively, whereas the dotted line indicates the time where ϕ_{PS^-} reaches unity.

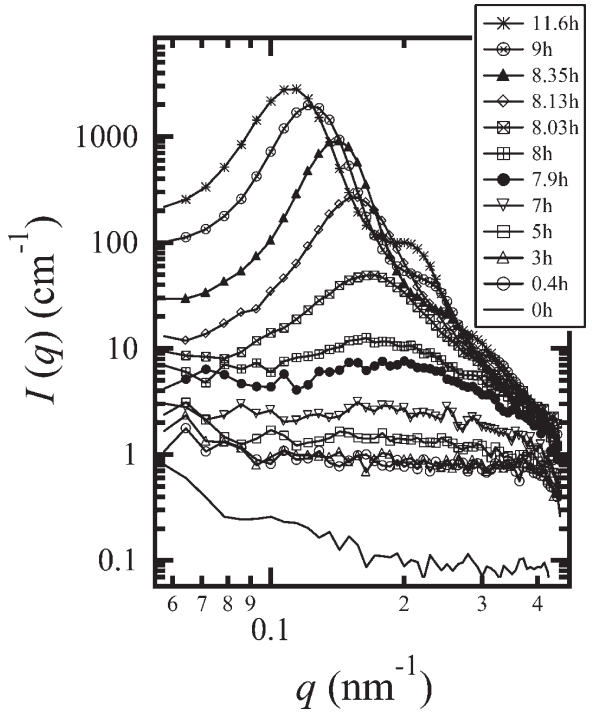

Figure 3. Time evolution of SANS profiles at different representative reaction times during the copolymerization process. The SANS profiles were corrected for incoherent scattering.

(= 0.5), which will be utilized later in conjunction with Figure 10.

Figure 1b shows time dependence of $M_{n,app}$, M_n, and M_w/M_n estimated from the SEC measurements. In region I, either $M_{n,app}$ or M_n rapidly increase in the early stage at $0 \le t/h \le 4$ (region I_a) and then slowly increase to an approximately steady value in the late stage at $4 \le t/h \le 7.8$ (region I_b). In region II, $M_{n,app}$ or M_n starts to rapidly increase again with time at $7.8 \le t/h \le 10$, followed by a slow increase to a final value. The observed two-step increase in $M_{n,app}$ or M_n with t is very consistent with the results previously reported for the simultaneous copolymerization.[16,20,21] As for M_w/M_n, at $t = 0.5$ h, the earliest accessible reaction time in this study, M_w/M_n is ~1.054. As the polymerization reaction proceeds, it slightly decreases to a constant value of 1.045, as expected. However, we find an increase in M_w/M_n from 1.045 at 7.8 h to 1.08 at 8.5 h and then a slow decrease to 1.055 in the end of region II.

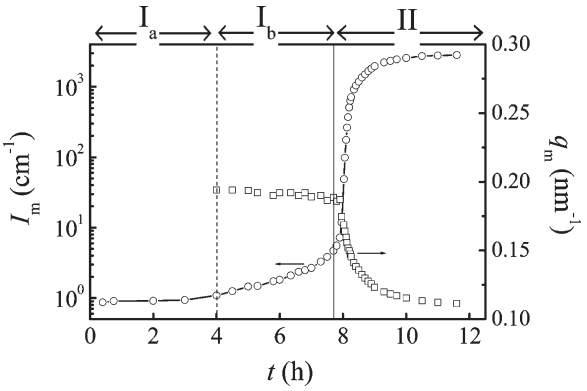

Figure 4. Time dependence of I_m and q_m during the copolymerization process. The vertical broken and solid lines indicate the time at the end of region I_a ($t_{c,SANS} \approx 4$ h) and region I_b ($t \approx 7.8$ h), respectively.

Figure 1c shows that the $M_{n,app}(t)$ linearly increases with the $C_T(t)$, indicating that the copolymerization follows the well-controlled living polymerization. Therefore, it is natural that the change in $M_{n,app}$ and C_T with t is identical, including the stepwise behavior.

III-2. Time-Resolved UV−vis Spectroscopy. Figure 2 shows time change in $A(450)$ during the polymerization process. Note that the solution before polymerization (t = 0), containing only *sec*-butyllithium and deuterated benzene, shows no absorption in the wavelength range covered in this study. Therefore, the absolute value of $A(450)$ was used directly for determinations of ϕ_{PS^-} in the following analysis. In region I, $A(450)$ is very small and almost independent of time, except for a slight but appreciable increase at the end of region I. In region II, it increases rapidly with time until $t \approx$ 8.5 h, beyond which it shows an almost constant value of $A_\infty(450) = 0.75$. Therefore ϕ_{PS^-} reaches unity, as shown in the right ordinate axis in Figure 2.

III-3. Time-Resolved SANS Measurement. Figure 3 shows Tr-SANS profiles at representative reaction times during the copolymerization process. The scattering profile before polymerization ($t = 0$) is also plotted in the same Figure as a reference (the solid line in the bottom of the Figure). It is weak and independent of q at $q > 0.15$ nm^{-1}, although a slight upturn with a decrease in q seemingly arising from the aggregates of the initiator is observed at low q region ($q <$ 0.15 nm^{-1}). In the early stage of region I (region I_a), the scattering profiles are nearly independent of q and hardly change with time. However, in the late stage of region I (region I_b) at $4 \le t/h \le 7.8$, a broad scattering peak appears. Although the scattering maximum, I_m, increases gradually with time, t, the peak position, q_m, changes little with t. The appearance of the scattering maximum, which motivated the classification of region I into I_a and I_b, is closely related to the time change in some reaction parameters: the increase in ϕ_{PS^-} (Figure 2) and the small increase in C_S from the level of 0.4 to 0.5 (Figure 1) with time and a sharp change in the sequence distribution P_I and P_S with time to be shown later in Figure 5, all in region I_b. In region II, I_m and q_m increase and decrease rapidly, respectively. In addition, the higher-order scattering peaks begin to show up with time.

Figure 4 shows the time evolution of I_m and q_m throughout the polymerization. At $0 < t/h < 4$, because no peak appears in any scattering profiles, we plot the scattering intensity at $q \approx 1.9$ nm^{-1} instead of I_m, where the scattering maximum began to show up at $t = 4$ h. At $0 < t/h < 4$ (region I_a), I_m keeps a constant value with time; at $4 < t/h \le 7.8$ (region I_b), I_m starts to increase slightly, but q_m appears to have a nearly constant value of ~1.9 nm^{-1} or to decrease slightly with t.

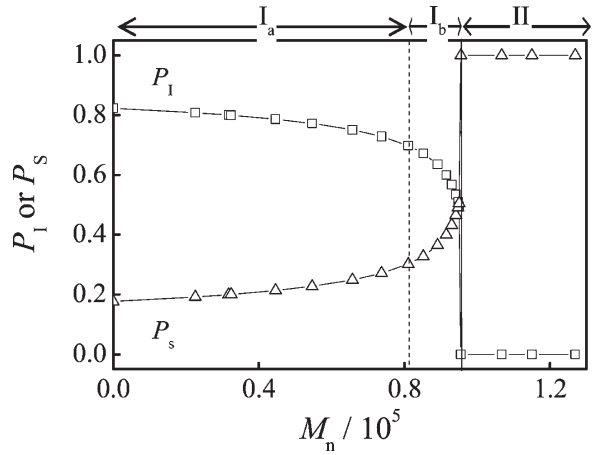

Figure 5. Average number fraction of I and S monomers (P_I and P_S, respectively) incorporated in a propagating copolymer chain as a function of M_n. The vertical broken and solid lines indicate the time at the end of region I_a ($t_{c,SANS} \approx 4$ h) and region I_b ($t \approx 7.8$ h), respectively.

In region II at $t > 7.8$ h, I_m and q_m rapidly increase and decrease, respectively. The details will be discussed in Section IV.

IV. Discussion

IV-1. Sequence Distribution of I and S Monomers in Propagating (Tapered Block) Copolymer Chains. It is known that the different reactivity ratio of S and I results in the formation of a tapered block copolymer.[5−9] The sequence distribution of I and S monomers along the tapered block chain affects its morphology[22−24] and physical properties.[22−26] The clarification of the sequence distribution simultaneously with other parameters is indispensable for deep insight into not only the copolymerization process, as will be discussed in the next section, but also physical properties of the copolymers. In this study, owing to the knowledge of $C_I(t)$ and $C_S(t)$, we are able to determine the average number fractions of I (P_I) and S (P_S) monomers incorporated along the propagating copolymer chain during the whole polymerization process.

Our earlier study confirmed that the copolymerization reaction of S and I initiated with *sec*-BuLi in nonpolar solvents approximately follows the first-order kinetics.[16] The approximation was also found to be well applicable to $C_I(t)$ and $C_S(t)$ well in this copolymerization reaction at the high monomer concentration, as shown in solid lines in Figure 1a. In region I, $C_I(t)$ and $C_S(t)$ could be expressed as follows, which will be detailed in Section IV-2

$$C_I = 1 - \exp(-R_I t); \quad R_I = (1.67 \pm 0.06) \times 10^{-4}\ \mathrm{s}^{-1} \quad (6)$$

$$C_S = 0.53 \times [1 - \exp(-R_S t)];$$
$$R_S = (1.12 \pm 0.1) \times 10^{-4}\ \mathrm{s}^{-1} \quad (7)$$

Therefore, the average number of I monomers, $r_I(t)$, and S monomers, $r_S(t)$, incorporated in the tapered block copolymer at a given t, is given by

$$r_I(t) = \frac{\mathrm{d}[N_{I,\mathrm{final}} C_I(t)]}{\mathrm{d}t}$$
$$= 933 \times 0.000167 \times \exp(-0.000167t) \quad (8)$$

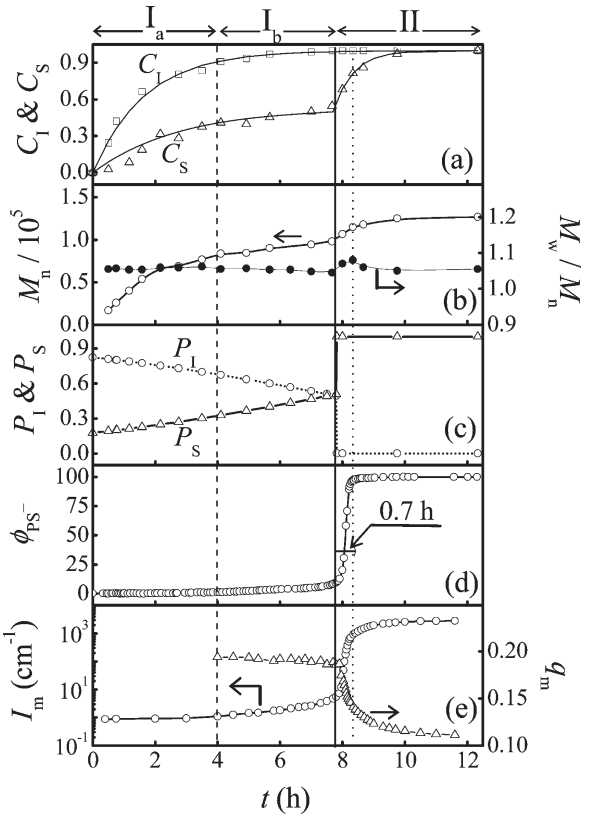

Figure 6. Summary of time dependence of the characteristic parameters plotted on the common time scale. (a) C_I and C_S, (b) M_n and M_w/M_n, (c) P_I and P_S, (d) ϕ_{PS^-}, and (e) I_m and q_m. The vertical broken and solid lines indicate the time at the end of region I_a ($t_{c,SANS} \approx 4$ h) and region I_b ($t \approx 7.8$ h), respectively, and the dotted line indicates the time where ϕ_{PS^-} reaches unity.

$$r_S(t) = \frac{\mathrm{d}[N_{S,\mathrm{final}} C_S(t)]}{\mathrm{d}t}$$
$$= 567 \times 0.53 \times 0.000112 \times \exp(-0.000112t) \quad (9)$$

in units of s^{-1}, where $N_{I,\mathrm{final}}$ and $N_{S,\mathrm{final}}$ are given by ref 19. Therefore, the average number fraction of I and S monomers, $P_I(t)$ and $P_S(t)$, incorporated to the copolymer at a given t are given by

$$P_I(t) = \frac{r_I(t)}{r_I(t) + r_S(t)} \quad (10)$$

$$P_S(t) = \frac{r_S(t)}{r_I(t) + r_S(t)} = 1 - P_I(t) \quad (11)$$

and the results will be shown later in Figure 6c. At the end of region II, $P_I(t)$ rapidly jumps down to 0 because of the complete consumption of I, whereas $P_S(t)$ jumps accordingly up to 1. Because $M_n(t)$ can be experimentally evaluated by eq 4, $P_I(t)$ or $P_S(t)$ versus t can be converted to P_I or P_S versus M_n, as shown in Figure 5. The vertical solid line and broken line indicate the end of regions I and I_a, respectively. In region I, the decrease in P_I and the increase in P_S were found as follows: (i) in the early stage of region I (region I_a), the chain has a small gradient of composition in either of the monomers, where P_I decreases from 0.82 to 0.67 and P_S increases from 0.18 to 0.33; (ii) in the late stage of region I (region I_b), a sharp gradient of composition in either of the monomers was observed, where P_I decreases from 0.67 to 0, and P_S increases from 0.33 to 1. This explains why the scattering maximum starts to appear in region I_b: the

copolymer can be approximated to be a block copolymer composed of a random copolymer and a short copolymer having a steep tapered composition gradient. In region II, $P_I \approx 0$ and $P_S \approx 1$ because of the absence of I monomers in the reaction solution. Therefore, pure PS block chains are formed in region II.

IV-2. Simultaneous Copolymerization Process and Mechanism As Observed by the Combined Time-Resolved Studies of Various Quantities Displayed on a Rigorously Common Time Axis. In this section, we discuss in detail the simultaneous copolymerization process and mechanism on the following three length scales: (i) mesoscopic structure of nanopatterns in terms of I_m and q_m, as observed by Tr-SANS, (ii) the primary structure of the single chains in terms of M_n and M_w/M_n, C_I or C_S, and P_I or P_S, as observed by SEC and NMR, and (iii) microscopic structure of the chain ends in terms of ϕ_{PS^-}, as observed by Tr-UV−vis. Comparisons of the time changes in all parameters mentioned above on the common time scale are indispensable to gain a deep understanding of the copolymerization process and mechanism, and thus they are shown together in Figure 6a−e, regardless of some redundancies.

Region I ($0 \le t/h \le 7.8$). C_I continuously increases with time up to 1.0, but C_S and M_n increase to almost constant values of 0.5 and 9.5×10^4, respectively. (See parts a and b in Figure 6.) P_I is always larger than P_S (part c), indicating that the incorporation of I into the propagating chain outweighs the incorporation of S, as predicted by eq 1, and is consistent with the previous reports.[4] M_w/M_n decreases slightly with time, as expected for living anionic polymerization. ϕ_{PS^-} remains very small except for the end of this region, indicating that a short lifetime of PS^- and hence almost all living chain ends are composed of PI^-. At the end of this region, $\phi_{PS^-} = 0.1$, $C_I = 1.0$, and $C_S = 0.5$. The result apparently means that 90 and 10% of the total living ends are occupied by PI^- and PS^- when 100% of I monomers and 50% of S monomers are consumed at the end of this region.

In region I, the following four propagation reactions occur[4]

$$(i)\ PI^- + I \rightarrow PI^-,\ \text{with}\ -d[I]/dt = k_{II}[PI^-][I] = R_{II}[I],\ \text{where}\ R_{II} \equiv k_{II}[PI^-] \quad (12a)$$

$$(ii)\ PI^- + S \rightarrow PS^-,\ \text{with}\ -d[S]/dt = k_{IS}[PI^-][S] = R_{IS}[S],\ \text{where}\ R_{IS} \equiv k_{IS}[PI^-] \quad (12b)$$

$$(iii)\ PS^- + I \rightarrow PI^-,\ \text{with}\ -d[I]/dt = k_{SI}[PS^-][I] = R_{SI}[I],\ \text{where}\ R_{SI} \equiv k_{SI}[PS^-] \quad (12c)$$

$$(iv)\ PS^- + S \rightarrow PS^-,\ \text{with}\ -d[S]/dt = k_{SS}[PS^-][S] = R_{SS}[S],\ \text{where}\ R_{SS} \equiv k_{SS}[PS^-] \quad (12d)$$

where k_{AB} and R_{AB} are the rate constant ($M^{-1}\ s^{-1}$) and the apparent reaction rate constant (s^{-1}), respectively, for the addition of B monomer to PA^- to give rise to PAB^-. [X] (X = I, S, PI^-, and PS^-) denotes the concentration of X. The total consumption rate or reaction rate of I, $-d[I]/dt$, is related to reactions 12a and 12c by

$$-d[I]/dt = R_I[I],$$

where

$$R_I = R_{II} + R_{SI} = k_{II}[PI^-] + k_{SI}[PS^-] = k_{II}K_I^{1/4}[(PI^-)_4]^{1/4} + k_{SI}K_S^{1/2}[(PS^-)_2]^{1/2} \quad (13a)$$

where K_I is the equilibrium constant of polyisoprenyl anion between tetramers and unimers, and K_S is the equilibrium constant of polystyryl anion between dimers and unimers

$$(PI^-)_4 \rightleftharpoons 4PI^-,\ K_I = [PI^-]^4/[(PI^-)_4] \text{ and } (PS^-)_2 \rightleftharpoons 2PS^-,\ K_S = [PS^-]^2/[(PS^-)_2] \quad (13b)$$

Here $(PI^-)_4$ and $(PS^-)_2$ designate the tetramer of PI^- and the dimer of PS^-, respectively, and $[(PI^-)_4]$ and $[(PS^-)_2]$ designate the corresponding concentration.

It is generally accepted that the homopolymerization reaction of S or I initiated with *sec*-BuLi in nonpolar solvent follows the first-order kinetics.[27] Our recent study showed that the copolymerization in dilute solutions follows the same kinetics as well.[16] The first-order kinetics is also found to fit approximately well in this concentrated copolymerization experiment, as shown by the good agreement between the experimental values (symbols) and the solid line in Figures 6a or 1a. To validate the first-order approximation, R_I in eq 13a should be a constant and independent of time. Actually, ϕ_{PS^-} in region I is almost constant, which implies that $[PI^-]$ and $[PS^-]$ and hence R_I are almost constant with time. This is why the first-order approximation works well for this copolymerization reaction. The same argument can be also applied to C_S, where C_S is given by eq 7. Moreover, R_I obtained from eq 6 is very close to the value, $R_{I,homo}$, for the homopolymerization of I [$R_{I,homo} = (1.71 \pm 0.07) \times 10^{-4}\ s^{-1}$] for the same total living anion concentration, the same solvent, and the same reaction temperature.[28,29] This result indicates that the contribution of the second term, $k_{SI}[PS^-]$, in eq 13a is really small, which seems reasonable because of the very small value of $[PS^-]$ and hence a very short lifetime of PS^- as a consequence of the large k_{SI} value.

In region I_b, the scattering maximum appears in the SANS profiles. (See Figure 6e.) The maximum arises from the correlation hole effect inherent in bcp's in the disordered state.[30,31] The appearance of this maximum occurs in parallel to the fact that ϕ_{PS^-} starts increasing with t, which in turn is a consequence of the increasing amount of S units incorporated in the propagating chains (P_S), as shown in part c from 30 to ~50 wt %. Although the fraction of I and S units incorporated into the chains, P_I and P_S, decreases and increases, respectively, almost at a constant rate in regions I_a and I_b, as shown in part c, molecular weight increases rapidly in region I_a, but the increase is slowed down in region I_b. This reveals that the tapered block chains formed have a small composition gradient along the chains in region I_a and a large composition gradient in region I_b, as clearly demonstrated in Figure 5. The creation of block sequence with the steeply tapered composition would give rise to the scattering maximum. However, the molecular weight increase in region I_b is small ($M_n = (8.4 \text{ to } 9.5) \times 10^4$), and hence the R_g of the propagating chains increases only a little, which accounts for the only a small decrease in q_m in region I_b.

It is interesting to see that I_m in region I_a hardly changes with time, as shown in Figure 6e. For correct interpretations of I_m versus t, it is important to know whether the propagating living chains are in dilute solutions or semidilute solutions. Therefore, let us estimate when the system attains the overlap concentration, c^*. We can estimate the time, t^*, and molecular weight, $M(t^*)$, or the degree of the polymerization (DP), $N(t^*)$, when the growing chains attain c^*, as follows. According to the definition, c^* is given by

$$c^* = \frac{M(t^*)}{N_A\left(\frac{4\pi}{3}R_g^3\right)} \quad (14)$$

Table 1. List of Characteristic Parameters Used in This Study[a]

X	X_I	X_S	$X_{I,m}$	$X_{S,m}$	X_B
ρ ($\times 10^{10}$ cm^{-2})	0.27	6.42	0.2	5.61	5.44
ν (cm^3/mol)	73.5	100	100	114.4	88.4
M (g/mol)	68	112	68	112	84
d (g/cm^3)	0.925	1.1	0.681	0.979	0.95

[a] X_K refers to one of the quantities X (X = ρ, ν, M, or d) for the Kth component [K = I, S, I,m (monomer I), S,m (monomer S), and benzene-d_6]. Besides the parameters in this Table, the value N_B is required (N_B = 1512).

where N_A is the Avogadro's number, $R_g(t)$ is the radius of gyration of the chain, assumed to be given by $R_g(t) = [N(t^*)a^2/6]^{1/2}$, where $N(t^*) = N_{I,final}C_I(t^*) + N_{S,final}C_S(t^*)$, with $N_{I,final}$ and $N_{S,final}$ being the total number of I and S monomeric unit per chain at the end of the polymerization, respectively, as detailed in ref 19, $C_I(t^*)$ and $C_S(t^*)$ being the I and S monomer conversions at t^*, respectively. Note that C_I and C_S approximately follow the first-order kinetics in this experiment, as given by eqs 6 and 7 in region I, which has been mentioned in Section IV-I. a is the averaged segment length (a = 0.68 nm).[32,33] Therefore, eq 14 is rewritten to

$$\frac{c^*}{M(t^*)} = \frac{1}{N_A\frac{4\pi}{3}\left[\frac{933\times(1-e^{-1.67\times10^{-4}t^*})\times0.68^2+567\times0.53\times(1-e^{-1.12\times10^{-4}t^*})\times0.68^2}{6}\right]^{3/2}} \quad (15)$$

The effective number of living polymer chains in the solution is constant given by

$$[\mathrm{Ini}]_{eff} = \frac{c^*}{M(t^*)} = 3.4\times10^{-3}\ \mathrm{M} \quad (16)$$

Therefore, t^* is calculated from eqs 15 and 16 to be ~0.53 h corresponding to only the beginning of region I_a. Actually, the propagating chains are expanded because of excluded-volume effects so that the solution may reach the overlap concentration at an earlier time than this time.

Under the given piece of evidence that the propagating chains form a semidilute solution in the very early stage of region I_a, let us now consider the behavior of I_m versus t in this region. The change in I_m may be due to a counterbalance of the following two factors. (i) I decreases with time because of the increase in polymer concentration, c, in a semidilute solution at $c > c^*$. I is given by $I \propto c^2\xi^3 \approx c^{-1/4} \propto M_n^{-1/4}$,[34] where ξ ($\sim c^{-3/4}$) denotes the thermal correlation length of the semidilute solution. Therefore, the increase in M_n of the propagating chains leads to a decrease in I. (ii) The scattering intensity at $q \approx 0$, $I(0)$, increases with time, because of the increase in the scattering contrast, $\Delta\rho^2$, because $I(0) \propto \Delta\rho^2$ according to the scattering theory,[35,36] where $\Delta\rho$ is defined by the difference of the scattering length density between the polymer chain, ρ_{polym}, and solvents, ρ_{solv}, given by

$$\rho_{polym} = \frac{\phi_I\rho_I+\phi_S\rho_S}{\phi_I+\phi_S} = P_I\rho_I + P_S\rho_S \quad (17)$$

$$\rho_{solv} = \frac{\phi_{I,m}\rho_{I,m}+\phi_{S,m}\rho_{S,m}+\phi_B\rho_B}{\phi_{I,m}+\phi_{S,m}+\phi_B} \quad (18)$$

where ϕ_X and ρ_X (X = I or deuterated S) in eq 17 denote the volume fraction and scattering length density of monomeric unit X in the copolymer chain, respectively. $\phi_{X,m}$ and $\rho_{X,m}$ (X = I or deuterated S) in eq 18 denote the volume fraction and scattering length density of X for the monomer in the reaction medium, respectively. ϕ_B and ρ_B in eq 18 denote the volume fraction and the scattering length density of benzene-d_6, respectively. ϕ_X and $\phi_{X,m}$ can also be calculated in terms of C_X as follows

$$\phi_X(t) = N_{X,\mathrm{final}}v_X C_X(t)/D(t) \quad (X = S \text{ or } I) \quad (19)$$

$$\phi_{X,m}(t) = N_{X,\mathrm{final}}v_{X,m}[1-C_X(t)]/D(t) \quad (X = I \text{ or } S) \quad (20)$$

with

$$D(t) = N_{S,\mathrm{final}}v_S C_S(t) + N_{I,\mathrm{final}}v_I C_I(t) + N_{S,\mathrm{final}}v_{S,m}[1-C_S(t)] + N_{I,\mathrm{final}}v_{I,m}[1-C_I(t)] + N_B v_B \quad (21)$$

where v_X or $v_{X,m}$ (X = deuterated S, I, or B) denote the molar volume of either monomeric units, monomers, or benzene-d_6, which could be estimated by $v_X = M_X/d_X$, where M_X and d_X are the molecular weight and density of X, respectively. N_B in eq 21 is the average number of benzene molecules per chain, which can be estimated from the composition of the system before the polymerization (t = 0), given by $N_B = (W_{B,t=0}/M_B)/((W_{S,m,t=0}+W_{I,m,t=0})/M_{n,final}) \approx 1512$, where $W_{B,t=0}$ and $W_{X,m,t=0}$ (X = deuterated S or I) denote the initial weight of benzene-d_6 and monomers X at t = 0, respectively. All parameters required for eqs 17−21 are summarized in Table 1. Therefore, ρ_{polym} and ρ_{solv} can be given by

$$\rho_{polym} = (0.27P_I + 6.42P_S)\times10^{10} \quad (22)$$

$$\rho_{solv} = \left[\frac{933\times100\times(1-C_I)\times0.2+567\times114.4\times(1-C_S)\times5.61+1512\times88.4\times5.44}{933\times100\times(1-C_I)+567\times114.4\times(1-C_S)+1512\times88.4}\right]\times10^{10} \quad (23)$$

Therefore, $\Delta\rho^2 = (\rho_{polym}-\rho_{solv})^2$ can be calculated by eqs 22 and 23. Taking both factors (i) and (ii) into account, $I(0)$ could be given by the product, $I(0) \approx \Delta\rho^2 M_n^{-1/4}$. The time-dependent parameter $\Delta\rho^2 M_n^{-1/4}$ and $\Delta\rho^2 M_n^{-1/4}$ in region I are shown in Figure 7a,b, respectively. An increase in $\Delta\rho^2$ and a decrease in $M_n^{-1/4}$ are clearly observed with t in Figure 7a, whereas $\Delta\rho^2 M_n^{-1/4}$ shows a constant value in Figure 7b. Consequently, the counterbalance of the two

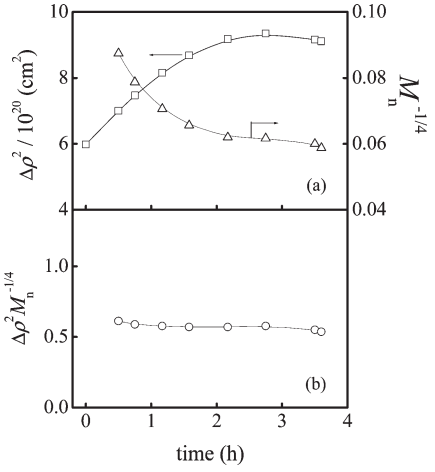

Figure 7. Time dependence of (a) $\Delta\rho^2$, M_n and (b) $\Delta\rho^2 M_n^{-1/4}$ in region I_a.

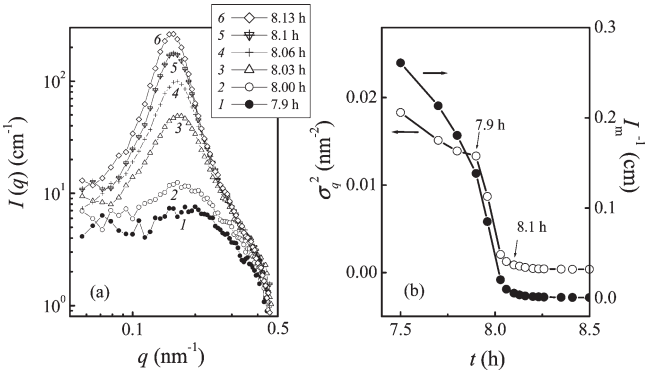

Figure 8. (a) Time-evolution of SANS profiles; (b) I_m^{-1} and σ_q^2 plotted as a function of t, both being focused on only around t_{ODT} for the reaction solution. Onset and completion time for ordering (disordering) at ODT are marked with the arrows in part b.

factors explains the fact that the observed I_m hardly changes with time in region I_a, although $M_n(t)$ increases with t.

Region II ($7.8 < t/h \leq 12$). P_I is always 0, whereas P_S is 1. Concurrently, ϕ_{PS^-} estimated from UV absorption at 450 nm starts to increase rapidly from ~10 to ~100% (Figure 6d). A change in the living chain end from PI^- to PS^- occurs over ~0.7 h in the beginning of region II (defined hereafter as an early stage of II), which is obviously due to the reaction of the living chain ends (either PI^- or PS^-) only with S monomers that remain in the system. This time span observed for the concentrated monomer system is much shorter than that observed for the dilute monomer system,[16] possibly because of the fact that the smaller effective anion concentration in the concentrated system (3.4 against 10.6 mM for the dilute system) results in a relatively weaker association power of $(PI^-)_4$ and hence a faster change from PI^- to PS^-.

C_S and M_n stepwisely increase in this region and reach the respective constant values because of the propagation of pure PS blocks. However, it is striking to note that a large fraction of PI^- ($\phi_{PI^-} \approx 90\%$) still survives in the beginning of region II despite the fact that I monomers are completely consumed. Similarly to our earlier study for the dilute solution,[16] the surviving PI^- may possibly form (i) the aggregates with association number, $n = 4$, and (ii) mixed aggregates with PS^- with n between 4 and 2, and these aggregates coexist with the PS^- aggregates with $n = 2$ in the early stage of region II.

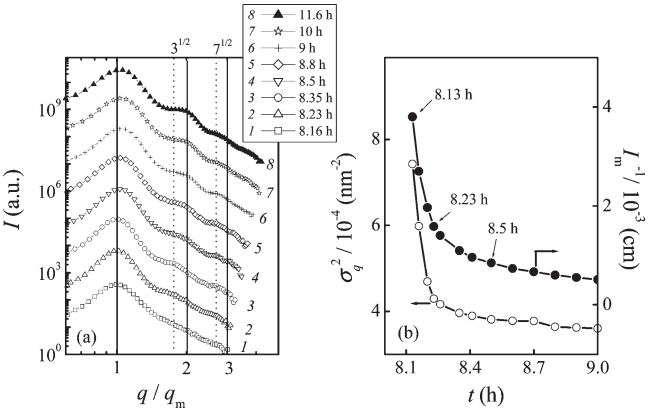

Figure 9. (a) Time-evolution of SANS profiles; (b) I_m^{-1} and σ_q^2 plotted as a function of t, both being focused on only after t_{ODT} and around t_{OOT} for the reaction solution. The SANS profiles were shifted vertically for clarity in part a. Onset times for disordered spheres, hexagonal cylinders, and alternating lamellae are marked with the arrows in part b.

We observe an increase in M_w/M_n in the early stage of region II, as shown in Figure 6b. As we discussed above, PI^- and PS^- coexist together in region II up to $t \approx 8.5$ h, during the period of which $[PI^-]$ decays to 0. In this time span, there may be a slow equilibration among dimers $(PS^-)_2$, tetramers $(PI^-)_4$, and mixed aggregates $(PI^-/PS^-)_x$ ($2 \leq x \leq 4$). The living chains having PS^- ends in the dimers will propagate fast, whereas the living chains having PS^- ends in the mixed aggregates or having PI^- ends in the tetramers will propagate slowly. The existence of living chains having PI^- ends in the tetramers and/or the mixed aggregates, as revealed by $(1 - \phi_{PS^-})$, simply means that these chains are not propagating. This offers the primary cause for the increase in M_w/M_n in this region. Later on, the effect of the PI^- survival in the beginning of region II becomes less important with time, and M_w/M_n tends to decrease slowly with t to a value ~1.055.

In region II, I_m and q_m rapidly increase and decrease with time, respectively, as shown in Figure 6e. The broad peak suddenly narrows, as shown in Figure 8a, and then appearance of the higher-order peaks at $3^{1/2}$ and $7^{1/2}$ positions of q_m is observed, as shown in Figure 9a, indicating that the order−disorder transition (ODT) occurred and the hexagonally packed cylindrical microdomains of dPS are formed in the matrix of PI. To characterize further ODT quantitatively, the first-order peak was analyzed in terms of its maximum intensity (I_m), peak position (q_m), and half-width at half-maximum (HWHM, σ_q). Conventionally, the plot of I_m^{-1} or σ_q^2 versus temperature, T, has been used to characterize the thermally induced ODT, and it usually shows a discontinuous change at ODT temperature, T_{ODT},[37−42] as a signature of the fluctuation-induced first-order phase transition. In this case, we try the plot of I_m^{-1} or σ_q^2 versus t to investigate the polymerization-reaction-induced ODT.

Figure 8 shows the time change in SANS profiles, $I(q, t)$, focused on only around the ODT time, t_{ODT} (part a), and I_m^{-1} and σ_q^2 plotted as a function of t (part b). A sharp discontinuous change appears in a narrow time range between 7.9 and 8.06 h for $I(q, t)$ and for both I_m^{-1} versus t and σ_q^2 versus t as well. As we expected, both I_m^{-1} and σ_q^2 versus t have similar behavior. Therefore, t_{ODT} is determined to be between 7.9 and 8.1 h in the time period of which the ordered state is expected to coexist with the disordered state. The polymerization-induced ODT also has the characteristic of the thermal-fluctuations-induced first-order transition. The ODT observed is considered to be a consequence of the

increasing DP of the pure PS block sequence from DP = 1257 (at 7.9 h) to 1322 (at 8.1 h). This fact also increases block copolymer concentration and the volume fraction of pure PS block in the propagating chain toward 1/2. All of these factors promote the ODT.

Figure 9a,b shows changes in the SANS profiles focused on only after t_{ODT} and I_m^{-1} and σ_q^2 with t for the first-order scattering peak, respectively. $I(q, t)$ was plotted against q/q_m to clarify the peak positions of the higher-order scattering peaks relative to that of the first-order peak in part a. Although the scattering profile at 8.13 h (profile 6 in Figure 8a) and that at 8.16 h (profile 1 in Figure 9a) do not show clearly the higher order scattering maxima inherent in the ordered bcp, the scattering profile at $t \approx 8.23$ and 8.35 h (profiles 2 and 3 in Figure 9a) clearly exhibits the second- and third-order peak at $3^{1/2}$ and $7^{1/2}$ q_m, typical of hexagonal cylinders. Therefore, in the time span between 8.13 and 8.23 h, PS spheres in the PI matrix are expected to be formed, although the higher-order peaks at $2^{1/2}$ and $3^{1/2}$ cannot be clearly identified in the scattering profiles because spheres may exist in a sufficiently disordered lattice. The transition between the disordered spheres and hexagonal cylinders was not accompanied by the discontinuous change in I_m^{-1} and σ_q^2 versus t but accompanied by the large changes in the values I_m^{-1} and σ_q^2, as shown in Figure 9b. The lack of long-range order in spheres (or spheres existing as the so-called disordered spheres)[43] may be partially due to the lack of the sufficient time required for spheres to order into bcc lattice or partially due to the ionic interactions at living chain ends that may destabilize the bcc spheres and stabilize the hexagonal cylinders.

The hexagonal cylinder is found to exist at 8.23 (profile 2) $\leq t/h <$ 8.8 (profile 5), as shown in Figure 9a. After 8.5 h, the higher-order peaks at integer-multiples of q_m are observed in Figure 9a, indicating that the polymerization-induced order−order transition (OOT) occurred from the hexagonally packed cylinders to the lamellar microdomains. The OOT also was not accompanied by the discontinuous changes in I_m^{-1} and σ_q^2 versus t. Note that both ODT and OOT in this experiment are a consequence of the increasing molecular weight of the PS block chains, volume fraction of PS, and the increasing polymer concentration. At OOT ($t \approx 8.5$ h), C_S and C_I are ~0.83 and 1.0, respectively, and thus the total volume fraction of S in one polymer chain at OOT, $\Phi_{S,OOT}$, can be calculated to be

$$\Phi_{S,OOT} = \frac{N_{S,final} C_S v_S}{N_{S,final} C_S v_S + N_{I,final} C_I v_I} = 0.41 \qquad (24)$$

where $N_{S,final}$ and $N_{I,final}$ are detailed in ref 19, and v_S and v_I are the molecular volume of S monomeric unit and I monomeric unit in a copolymer chain, respectively, as shown in Table 1. On the basis of the self-consistent mean-field theory,[44−46] the OOT from the hexagonally packed cylinders to the lamellar microdomains usually occurs at $\Phi_{S,OOT} \approx 0.33$ for the neat PS-*b*-PI bcp's. The much larger value of $\Phi_{S,OOT}$ found in this study is due to the formation of tapered block copolymers. It is intriguing to note that Tr-SANS measurements together with the evaluation of monomer conversions as a function of time offer an opportunity to investigate the building-up process of the primary molecular structure together with their bottom-up self-assembling processes during the polymerization.

It should be noted that the microdomain structure of the block copolymers depends not only on the volume fraction of constituent block chains, Φ, but also on χDP, where χ is the Flory−Huggins segmental interaction parameter and DP is the total degree of polymerization. The copolymers exhibit the OOT when Φ and χDP changed. In this study, during the polymerization, both Φ and χDP changed in a short time relative to the time required for the system to attain the equilibrium morphologies of the bcc sphere and the double gyroid with Ia$\bar{3}$d space group symmetry. To observe an equilibrium morphology during the polymerization, the reaction rate must be much smaller than the ordering rate. The following two methods might be applied to confirm the bcc and gyroid morphology: (1) prescribe an amount of S to prepare bcc or gyroid morphology at the end of the polymerization; and (2) perform a polymerization in which the propagating reaction rate is much smaller than the ordering rate of the bcc and gyroid morphology. The experiments mentioned above might be able to offer us a chance to follow OOT kinetics during the polymerization.

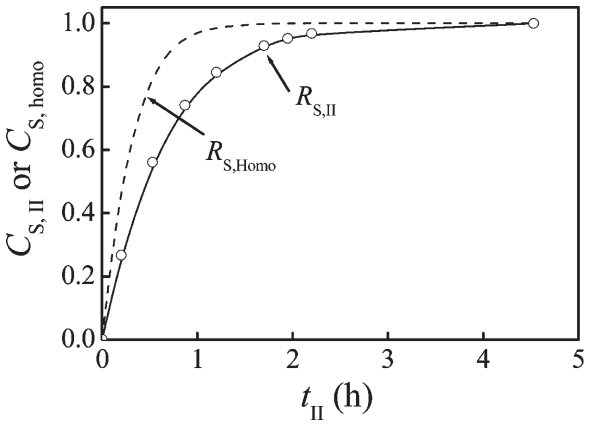

Figure 10. Comparison of monomer conversions of S in region II of our system (solid line) and that in the homopolymerization system (broken line) under the same polymerization conditions specified in the text.

IV-3. Comparison between the Rate of Block Copolymerization of Styrene in Region II and the Rate of Homopolymerization of S. Because in region II, only S monomers exist in the reaction solution, we expect that the polymerization of pure S monomers to pure PS block chains occurs under the influence of the PI^- living chain ends. Therefore, it is worthy to compare the polymerization rate of S to the PS block with the homopolymerization rate of S to homo PS under the same reaction conditions, such as the temperature (25 °C), solvent (benzene-d_6), and concentration of living chains (3.4 mM). This is because the comparison will clarify the effects of transformation of the chain-end aggregates from $(PI^-)_n$ to $(PS^-)_m$ on the reaction rate of S into PS^-. To do so, we should first separate the contribution of C_S value ($C_{S,r}$) at the end of region I from the net C_S value in region II by introducing a reduced monomer conversion of styrene in region II, $C_{S,II}$, defined by $C_{S,II} = (C_S - C_{S,r})/(1 - C_{S,r})$, and reduced time, t_{II}, defined by $t_{II} = t - t_r$, where $C_{S,r}$ and t_r are monomer conversion of S and the time at which all I monomers are effectively consumed, which have been already defined in Figure 1. Then, we plot $C_{S,II}$ versus t_{II} in Figure 10.

The time dependence of monomer conversion of S in the homopolymerization, $C_{S,homo}$, is also shown with the broken line in Figure 10 as a reference.[28,29] The first-order kinetics approximation works well for both the copolymerization and the homopolymerization, which is characterized by

$$C_{S,II} = 1 - \exp(-R_{S,II} t_{II}),$$
$$R_{S,II} = (4.3 \pm 0.2) \times 10^{-4}\ s^{-1} \qquad (25)$$

Table 2. Comparison between the Reaction Rates in the Concentrated Solution and Those in the Dilute Solution

monomers	obsd reaction rate ($\times 10^4$) s^{-1}		ratio[c]	
	concentrated solution[a]	dilute solution[b]	obsd[d]	pred[e]
isoprene	1.67 ± 0.06 (region I, eq 6)	2.25 ± 0.11 (region I, eq 14, ref 16.)	1.35	1.33[f]
styrene	1.12 ± 0.1 (region I, eq 7)	1.60 ± 0.14 (region I, eq 15, ref 16.)	1.43	1.33[f]
	4.3 ± 0.2 (region II, eq 25)	5.83 ± 0.8 (region II, eq 16, ref 16.)	1.35	1.25[g]

[a] Anion concentration ~3.4 mM. [b] Anion concentration ~10.6 mM. [c] (Reaction rate in the dilute solution)/(Reaction rate in the concentrated solution). [d] Observed ratio of c. [e] Predicted ratio calculated from eqs VI and VII in ref 28. [f] Prediction is based on the assumptions: (i) $(PI^-)_4 \rightleftharpoons 4PI^-$ and (ii) PI^- being active for the polymerization. [g] Prediction is based on the assumptions: (i) $(PS^-)_2 \rightleftharpoons 2PS^-$ and (ii) PS^- being active for the polymerization. In the case of the concentrated solution, the prediction utilizes the effective anion concentration $[PS^-]_{eff} = 6.8$ mM rather than the nominal anion concentration $[PS^-]_{nom} = 3.4$ mM.

for the copolymerization as shown by the solid line and by

$$C_{S,\,homo} = 1 - \exp(-R_{S,\,homo}t),$$

$$R_{S,\,homo} = (1.08 \pm 0.10) \times 10^{-3}\ s^{-1} \qquad (26)$$

for the homopolymerization, as shown by the broken line. A much slower reaction rate in the copolymerization system than that in the homopolymerization is found: $R_{S,II}$ is smaller than $R_{S,homo}$ by ~2.5 times. Note that the reaction rate may be accelerated because of the polymerization reaction in the microphase-separated domains, which may confine PS^- in PS microdomains, compared with a homogeneous distribution of PS^- in the solution in the case of homopolymerization. The microphase separation actually increases the local concentration of $[PS^-]$. If one simply takes a lamellar microdomain having $\Phi_S \approx 0.5$ into account, then the effective concentration, $[PS^-]_{eff}$, is estimated to be about double the nominal concentration, so that $[PS^-]_{eff} \approx 6.8$ mM instead of 3.4 mM. The corresponding $R_{S,homo}$ is $\sim 1.4 \times 10^{-3}\ s^{-1}$;[28,29] therefore, $R_{S,II}$ is actually smaller than $R_{S,homo}$ by ~3 times, which is consistent with our earlier report in the dilute system (section V-3 in ref 16), where microphase separation never occurs. The suppression of the reaction rate might be explained by a long life of PI^- living chain ends in region II, which may keep the chain end associations even under the situation where the PI^-s are surrounded only by S monomers. The chain ends associations $(PI^-)_4$ are expected to coexist with the mixed aggregates $(PI^-/PS^-)_x$ $(2 \le x \le 4)$ and $(PS^-)_2$, even after the complete consumption of I monomers, as evidenced by the change in ϕ_{PS^-} in the beginning of region II. The long life of $[PI^-]$ in region II reduces the concentration of PS^- unimers, $[PS^-]$, compared with those in the corresponding homopolymerization and hence suppresses the reaction rate of S.

IV-4. Comparison between the Reaction Rates of Copolymerizations in the Concentrated Monomer Solution and Those in the Dilute Monomer Solution. We like to compare the reaction rates of the copolymerization in the concentrated solution, as studied in this work, and those in the dilute solution, as reported in ref 16. The reaction rates for either I or S monomers in both cases are summarized in Table 2. To make a clear comparison, the observed and predicted ratios of the reaction rate in the dilute solution to that in the concentrated solution are also listed. Note that in region I, the prediction is based on the following two assumptions: (i) $(PI^-)_4 \rightleftharpoons 4PI^-$ and (ii) PI^- unimer being active for the polymerization, whereas in region II, it is based on the assumptions as: (i) $(PS^-)_2 \rightleftharpoons 2PS^-$ and (ii) PS^- unimer being active for the polymerization. In the case of the concentrated solution, $R_{S,II}$ in microdomains is accelerated by the fact that the effective anion concentration, $[PS^-]_{eff}$, in the lamellar microdomains is larger than the nominal anion concentration, $[PS^-]_{nom}$, by a factor of ~2; therefore, $[PS^-]_{eff} \approx 6.8$ mM rather than $[PS^-]_{nom} \approx 3.4$ mM should be utilized[28,29] to calculate the predicted ratio.The observed ratios were evaluated only from the experimental results determined on the basis of the approximation of the first-order reaction kinetics (eqs 6 and 7).

The observed ratios agree well with the predicted values, indicating that our assumption of existence of $(PI^-)_4$ and $(PS^-)_2$, which has been verified in the dilute solutions,[16] is reasonable in the concentrated solution also. Both the dilute and concentrated solutions are resemblant in nature, and thus the reaction kinetics could be deduced from one another by taking account of the difference in the living anion concentrations and the effects of the lamellar microdomain formation. Hence, the discussion on the association number, n, in ref 16 can be applied here in this study as well, although the direct evaluation of n, as we did in ref 16, is not possible for the concentrated solution because of the chain overlaps. Note that even in this case, the "random phase approximation" analysis on the star-shaped tapered block copolymers in the disordered state allows us to estimate n up to the end of region I, which will be reported in a companion paper.[47]

V. Concluding Remarks

As an extension of our previous work,[16] the living anionic copolymerization of a mixture of isoprene (I) and deuterated styrene (S) monomers in a concentrated monomer solution with benzene-d_6 as a non-polar solvent was investigated by simultaneous measurements of time-resolved SANS, SEC, NMR, and ultraviolet−visible (UV−vis) spectroscopy. The combined time-resolved methods were conducted on the same single-batch reaction solution, and hence we were able to investigate the structural change of the propagating living chains from the microscopic structure to the primary structure of single living chains and even to the high-order self-assembly or nanopatterns of the living chains formed via order−disorder transition and order−order transition.

The copolymerization process is divided into two time regions: In region I, the copolymerization of S and I monomers occurred, and all I monomers were consumed at the end of region I. In the early stage of region I (region I_a), the scattering intensity, I_m, hardly changed with time, whereas in the late stage of region I (region I_b), a scattering maximum appeared because of the increasing amount of S units incorporated in the propagating chains. In region II, pure polystyrene (PS) block chains were formed, and the polymerization-induced disorder−order transition and order−order transition were clearly observed from the change in SANS profiles. The living polymer chain ends started to change from PI^- into PS^- in this time span.

The comparison between the reaction rates of copolymerization in the concentrated monomer solution and those in the dilute monomer solution indicates that even in the concentrated solution, tetramers $(PI^-)_4$ exist in region I, and PI^- unimers are active in the polymerization, whereas in the early stage of region II, the mixed aggregates $(PI^-/PS^-)_x$ $(2 < x < 4)$ and dimers $(PS^-)_2$ coexist together and results in an increase in M_w/M_n. In the late stage of region II, dimers $(PS^-)_2$ survive, and PS^- unimers are the

active anions in the polymerization. The reaction rate, $R_{S,II}$, of S monomers to pure PS blocks in microdomains in region II is accelerated by the fact that the effective anion concentration is approximately doubled to the nominal anion concentration due to the microphase separation which confines the PS in the PS microdomains. This is another example showing that physics plays an important role for the chemical reaction in building up the specific reaction field.

The methodology to extract simultaneously, in situ and at real time, the various fundamental quantities during the course of the living anionic copolymerization process on a given batch of reaction solution again proves itself as a powerful way to study various polymerization systems, including living anionic polymerizations,[15,16] controlled radical polymerizations,[48,49] and so on. It offers us an opportunity to observe the time evolution of changes in different hierarchical structure levels from microscopic to mesoscopic structures and to explore the information transmittance among different hierarchical structure levels.

References and Notes

(1) Yamauchi, K.; Hasegawa, H.; Tanaka, H.; Motokawa, R.; Koizumi, S.; Hashimoto, T. *Macromolecules* **2006**, *39*, 4531–4539.
(2) Stellbrink, J.; Willner, L.; Richter, D.; Lindner, P.; Fetters, L. J.; Huang, J. S. *Macromolecules* **1998**, *31*, 4189−4197; *Macromolecules* **1999**, *32*, 5321−5329.
(3) Szwarc, M.; Van Beylen, M. *Ionic Polymerization and Living Polymers*; Chapman & Hall: New York, 1993.
(4) Worsfold, D. J. *J. Polym. Sci., Part A* **1967**, *5*, 2783–2789.
(5) Zelinski, R. P. U.S. Patent 2975160, **1961**.
(6) Kraus, G.; Childers, C. W.; Gruver, J. T. *J. Appl. Polym. Sci.* **1967**, *11*, 1581–1591.
(7) Kraus, G.; Rollmann, K. W. *Angew. Makromol. Chem.* **1971**, *16*/*17*, 271–296.
(8) Hsieh, H. L. In *Block and Graft Copolymers*; Burke, J. J., Weiss, V., Eds.; Syracuse University Press: Syracuse, NY, 1973.
(9) Aggarwal, S. L.; Livigni, R. A.; Marker, L. F.; Dudek, J. J. In *Block and Graft Copolymers*; Burke, J. J., Weiss, V., Eds.; Syracuse University Press: Syracuse, NY, 1973.
(10) Worsfold, D. J.; Bywater, S. *Macromolecules* **1972**, *5*, 393–397.
(11) Maliakal, A.; Greenaway, H.; Oshaughnessy, B.; Turro, N. J. *Macromolecules* **2003**, *36*, 6075–6080.
(12) Stellbrink, J.; Allgaier, J.; Willner, L.; Richter, D.; Slawecki, T.; Fetters, L. J. *Polymer* **2002**, *43*, 7101–7109.
(13) Fetters, L. J.; Balsara, N. P.; Huang, J. S.; Jeon, H. S.; Almdal, K.; Lin, M. Y. *Macromolecules* **1995**, *28*, 4996–5005.
(14) Niu, A. Z.; Stellbrink, J.; Allgaier, J.; Willner, L.; Radulescu, A.; Richter, D.; Koenig, B. W.; May, R. P.; Fetters, L. J. *J. Chem. Phys.* **2005**, *122*, 134906.
(15) Miyamoto, N.; Yamauchi, K.; Hasegawa, H.; Hashimoto, T.; Koizumi, S. *Physica B* **2006**, *385*, 752–755.
(16) Zhao, Y.; Tanaka, H.; Miyamoto, N.; Koizumi, S.; Hashimoto, T. *Macromolecules* **2009**, *42*, 1738–1748.
(17) Because some amount of initiators always become inactive due to the presence of impurities, in this study, we calculated the effective initiator concentration and compared it with the fed initiator concentration to check if the polymerization process is well controlled or not. The effective initiator concentration is calculated as $[\mathrm{Ini}]_{\mathrm{eff}} = W_{\mathrm{ini}}/(V_{\mathrm{total}}M_{\mathrm{n,final}}) = 3.4$ mM, where W_{ini} represents the total weight of fed monomers (4.33 g) per total volume of the reaction system, $V_{\mathrm{total}} = (50 \times 10^{-6} + 3.2 \times 10^{-3} + 2.2 \times 10^{-3} + 4.6 \times 10^{-3})\mathrm{L} = 10.05 \times 10^{-3}$ L (431 g/L) before the polymerization, and $M_{\mathrm{n,final}}$ represents the total molecular weight after the polymerization and termination ($\sim 1.27 \times 10^5$), as will be detailed in ref 19. The theoretical initiator concentration, $[\mathrm{Ini}]_{\mathrm{theor}}$, can be calculated from the fed initiator amount as $[\mathrm{Ini}]_{\mathrm{theor}} = n_{\mathrm{ini}}/V_{\mathrm{total}} \approx 5$ mM, where n_{ini} is moles of the fed initiator (50 μL solution of 1.0 M *sec*-BuLi).
(18) Koizumi, S.; Iwase, H.; Suzuki, J.; Oku, T.; Motokawa, R.; Sasao, H.; Tanaka, H.; Yamaguchi, D.; Shimizu, H. M.; Hashimoto, T. *J. Appl. Crystallogr.* **2007**, *40*, s474–s479.
(19) From SEC, the "apparent" number-average molecular weight of the copolymer chain, $M_{\mathrm{n,app}}$, can be calculated directly on the basis of polystyrene standard calibration. However, we must take into account the size difference between I and S monomeric units in the copolymer to estimate the true molecular weight M_{n} from $M_{\mathrm{n,app}}$. For this purpose, we used a calibration factor of 1.6 estimated for homoPI. This factor 1.6 was determined by measuring $M_{\mathrm{n,PI,app}}$ values by SEC with PS standard for a series of PI homopolymers having different $M_{\mathrm{n,PI}}$ values that were independently measured by a membrane osmometer. We assume that the factor of 1.6 is applicable to the copolymer also. We further assume that the "apparent" number-average molecular weight per copolymer chain at the end of polymerization, $M_{\mathrm{n,final,app}}$ ($\sim 1.64 \times 10^5$), can be expressed as follows

$$M_{\mathrm{n,\,final,\,app}} = 1.6 M_{\mathrm{I}} N_{\mathrm{I,\,final}} + M_{\mathrm{S}} N_{\mathrm{S,\,final}} \approx 1.64 \times 10^5 \qquad \text{(I)}$$

where M_{X} (X = I or S) is the molecular weight of X monomeric unit and $N_{\mathrm{X,final}}$ (X = I or S) is the number of X monomeric unit per chain at the end of the polymerization and after the termination of the living polymer. It should be noted that there is no theory that supports this assumption; however, there is no better way to handle the problem of determining molecular weight of the copolymers. Therefore we use this assumption to obtain an approximate values for $M_{\mathrm{n,final}}$. The initial monomer feeding ratio is known to be 50:50 wt %, therefore,

$$M_{\mathrm{I}} N_{\mathrm{I,\,final}} = M_{\mathrm{S}} N_{\mathrm{S,\,final}} \qquad \text{(II)}$$

From eqs I and II, $N_{\mathrm{I,final}} = 933$ and $N_{\mathrm{S,final}} = 567$. The true number-average molecular weight of the copolymer at the end of the polymerization and after the termination, $M_{\mathrm{n,final}}$, is therefore given by

$$M_{\mathrm{n,\,final}} = M_{\mathrm{I}} N_{\mathrm{I,\,final}} + M_{\mathrm{S}} N_{\mathrm{S,\,final}} \approx 1.27 \times 10^5 \qquad \text{(III)}$$

The true number-average molecular weight of I monomeric units and S monomeric units in one copolymer chain at the end of the polymerization and after the termination, $M_{\mathrm{n,final,I}}$ and $M_{\mathrm{n,final,S}}$ are given by

$$M_{\mathrm{n,\,final,\,I}} = M_{\mathrm{I}} N_{\mathrm{I,\,final}} \approx 6.35 \times 10^4 \qquad \text{(IV)}$$

$$M_{n,\,final,\,S} = M_{\mathrm{S}} N_{\mathrm{S,\,final}} \approx 6.35 \times 10^4 \qquad \text{(V)}$$

(20) Tanaka, Y.; Sato, H.; Nakafutami, Y.; Kashiwazaki, Y. *Macromolecules* **1983**, *16*, 1925–1928.
(21) Korotkov, A. A.; Rakova, G. V. *Vysokomol. Soedin.* **1961**, *10*, 1482–1490.
(22) Tsukahara, Y.; Nakamura, N.; Hashimoto, T.; Kawai, H.; Nagaya, T.; Sugimura, Y.; Tsuge, S. *Polym. J.* **1980**, *12*, 455–466.
(23) Hashimoto, T.; Tsukahara, Y.; Kawai, H. *Polym. J.* **1983**, *15*, 699–711.
(24) Hashimoto, T.; Tsukahara, Y.; Tachi, K.; Kawai, H. *Macromolecules* **1983**, *16*, 648–657.
(25) Hodrokoukes, P.; Floudas, G.; Pispas, S.; Hadjichristidis, N. *Macromolecules* **2001**, *34*, 650–657.
(26) Hodrokoukes, P.; Pispas, S.; Hadjichristidis, N. *Macromolecules* **2002**, *35*, 834–840.
(27) Hsieh, H. L. *J. Polym. Sci., Part A* **1965**, *3*, 153–161.
(28) The homopolymerization rates of I, $R_{\mathrm{I,homo}}$, as a function of [PI$^-$] and those of S, $R_{\mathrm{S,homo}}$, as a function of [PS$^-$] in benzene at 25 °C were determined by[29]

$$\log R_{\mathrm{I,\,homo}} \cong 0.25 \times \log[\mathrm{PI}^-] - 3.15 \qquad \text{(VI)}$$

$$\log R_{\mathrm{S,\,homo}} \cong 0.4 \times \log[\mathrm{PS}^-] - 1.98 \qquad \text{(VII)}$$

where the units for $R_{\mathrm{X,homo}}$ and [PX$^-$] (X = I or S) are s^{-1} and M, respectively. According to these two equations, $R_{\mathrm{I,homo}} = 1.71 \times 10^{-4}\ \mathrm{s}^{-1}$ and $R_{\mathrm{S,homo}} = 1.08 \times 10^{-3}\ \mathrm{s}^{-1}$ at the anion concentration of [PX$^-$] = 3.4 mM, which is the same total anion concentration as the copolymerization reaction in this study.
(29) Miyamoto, Y.; Koizumi, S.; Hashimoto, T., paper in preparation.
(30) Leibler, L. *Macromolecules* **1980**, *13*, 1602–1617.
(31) de Gennes, P. G. *Scaling Concepts in Polymer Physics*; Cornell University Press: Ithaca, NY, 1979.
(32) Ballard, D. G. H.; Wignall, G. D.; Schelte, J. *Eur. Polym. J.* **1973**, *9*, 965–969.

(33) Petychakis, L.; Floudas, G.; Fleischer, G. *Europhys. Lett.* **1997**, *40*, 685–690.
(34) Teraoka, I. *Polymer Solutions*; John Wiley & Sons Press: New York, 2002.
(35) Roe, R. J. *Methods of X-ray and Neutron Scattering in Polymer Science*; Oxford University Press: New York, 2000.
(36) Higgins, J. S.; Benoit, H. C. *Polymers and Neutron Scattering*; Clarendon Press: Oxford, U.K., 1994.
(37) Bates, F. S.; Rosedale, J. H.; Fredrickson, G. H. *J. Chem. Phys.* **1990**, *92*, 6255–6270.
(38) Stühn, B.; Mutter, R.; Albrecht, T. *Europhys. Lett.* **1992**, *18*, 427–432.
(39) Wolff, T.; Burger, C.; Ruland, W. *Macromolecules* **1993**, *26*, 1707–1711.
(40) Hashimoto, T.; Ogawa, T.; Han, C. D. *J. Phys. Soc. Jpn.* **1994**, *63*, 2206–2214.
(41) Floudas, G.; Pakula, T.; Fischer, E. W.; Hadjichristidis, N.; Pispas, S. *Acta Polym.* **1994**, *45*, 176–181.
(42) Sakamoto, N.; Hashimoto, T. *Macromolecules* **1995**, *28*, 6825–6834.
(43) Han, C. D.; Vaidya, N. Y.; Kim, D.; Shin, G.; Yamaguchi, D.; Hashimoto, T. *Macromolecules* **2000**, *33*, 3767–3780.
(44) Matsen, M. W.; Schick, M. *Macromolecules* **1994**, *27*, 6761−6767; *Macromolecules* **1994**, *27*, 7157−7163.
(45) Matsen, M. W.; Bates, F. S. *Macromolecules* **1996**, *29*, 1091–1098.
(46) Bates, F. S.; Fredrickson, G. H. *Phys. Today* **1999**, *52*, 32.
(47) Zhao, Y.; Kawakatsu, T.; Koizumi, S.; Hashimoto, T., paper in preparation.
(48) Motokawa, R.; Iida, Y.; Zhao, Y.; Hashimoto, T.; Koizumi, S. *Polym. J.* **2007**, *39*, 1312–1318.
(49) Motokawa, R.; Koizumi, S.; Zhao, Y.; Hashimoto, T. *J. Appl. Crystallogr.* **2007**, *40*, S645–S649.